Nuclear Inst. and Methods in Physics Research, A 934 (2019) 41–51

Contents lists available at ScienceDirect

Nuclear Inst. and Methods in Physics Research, A

journal homepage: www.elsevier.com/locate/nima

Reconstruction method for gamma-ray coded-aperture imaging based on convolutional neural network

Rui Zhang [a], Pin Gong [a,b], Xiaobin Tang [a,b,*], Peng Wang [c], Cheng Zhou [d], Xiaoxiang Zhu [d], Le Gao [a], Dajian Liang [a], Zeyu Wang [a]

[a] Department of Nuclear Science and Engineering, Nanjing University of Aeronautics and Astronautics, Nanjing 210016, China
[b] Jiangsu Engineering Laboratory of Nuclear Energy Equipment Materials, Nanjing University of Aeronautics and Astronautics, Nanjing 210016, China
[c] School of Environmental and Biological Engineering, Nanjing University of Science and Technology, Nanjing 210094, China
[d] Jiangsu Nuclear and Radiation Safety Supervision and Management Center, Nanjing 210019, China

ARTICLE INFO

Keywords:
Coded-aperture imaging
Gamma camera
Convolution neural network
Monte Carlo simulation

ABSTRACT

Coded-aperture gamma-ray imaging has great application value in the fields of nuclear security, nuclear facility decommissioning, and decontamination verification. However, conventional reconstruction methods cannot handle the signal-independent noise. In this paper, a coded-aperture imaging reconstruction method based on convolutional neural network (CNN) was proposed to improve the performance of image reconstruction and enhance the source position recognition ability of imaging systems. In addition, a compact gamma camera based on cadmium zinc telluride (CZT) pixel detector and uniformly redundant array (MURA) mask was modeled. Monte Carlo simulation data were used to train CNN and test the performance of this method. Furthermore, the reconstruction of the CNN method and the correlation analysis method with different radioactive sources and measurement conditions were compared. Results show that the proposed method can suppress the reconstructed image noise well. The reconstructed images have higher contrast-to-noise ratio (CNR) than the correlation analysis method in radioactive source location.

Contents

1. Introduction

Radioactive source, reactor, and irradiation devices have been employed in various fields of industrial production. In this respect, nuclear security and safety has become a great challenge [1–3]. Accurate localization and identification of radioactive materials is crucial in

* Corresponding author at: Department of Nuclear Science and Engineering, Nanjing University of Aeronautics and Astronautics, Nanjing 210016, China.
E-mail address: tangxiaobin@nuaa.edu.cn (X. Tang).

https://doi.org/10.1016/j.nima.2019.04.055
Received 29 November 2018; Received in revised form 8 April 2019; Accepted 13 April 2019
Available online 4 May 2019
0168-9002/

the search for orphan radioactive sources [4], nuclear facility decontamination and decommissioning [5,6]. A coded-aperture gamma camera is capable of intuitively giving the radioactive distribution, providing a direct and accurate reference for localization of radioactive hot spots [7–11]. Unlike the single-pinhole imaging method, the coded-aperture approach introduces a multi-hole mask to improve the photon pass rate and signal-to-noise ratio (SNR) of images [1,12–15]. This approach reduces imaging time and radiation risk and improves work efficiency. In nuclear fuel plants and reactors, a coded-aperture gamma camera can provide great assistance in identifying radioactive leaks and contamination of pipelines [7,9]. In addition, a coded-aperture gamma camera can provide radiation pollution distributions and decontamination verifications in areas of nuclear accidents [16,17].

Conventional reconstruction methods of coded-aperture imaging include correlation analysis method and iterative decoding algorithm [18,19]. In the first case, the correlation analysis method can acquire a theoretical optimal reconstructed image by choosing the encoding and decoding arrays of which correlation approximates a delta function [12]. In the actual imaging process, the reconstructed image contains a considerable amount of noise from photon scattering and transmission, statistical fluctuation, and detector systems. However, the correlation analysis method cannot reduce noise and can only improve the quality of reconstruction by increasing exposure time [1]. The correlation analysis method has strict requirements for the design of the encoding array, thereby limiting the flexibility of the encoding mask design. In the other case, iterative decoding methods such as maximum entropy methods (MEM) [20] or maximum-likelihood expectation maximization (MLEM) algorithm [21,22] can greatly improve the reconstructed image. However, the reconstruction is much slower and requires high computing power, even in the simplest cases, thereby hindering large-scale array and real-time measurement.

Considering the remarkable progress has been achieved in computer science and neuroscience research over the past decades, artificial neural networks and deep learning methods [23] have been successfully applied to many nuclear technologies such as energy spectrum analysis and nuclide identification [24–26]. Back-propagation neural network has been used to simulate the MLEM algorithm in coded-aperture imaging, which speeded calculation in large array obviously [27]. Convolutional neural network (CNN) is the state-of-the-art function approximators for computer vision problems and is well suited for the deconvolution task [28,29], which means it possesses enough computational capacity to process reconstruction, including noise suppression in coded-aperture imaging.

To accelerate the acquisition of low noise reconstructed images, a reconstruction method based on CNN was proposed. A compact gamma camera based on a cadmium zinc telluride (CZT) pixel detector was built in the Particle and Heavy Ion Transport code System (PHITS) [30] to simulate the gamma-ray imaging process and obtain a training set for CNN. Reconstructions of the trained CNN and the correlation analysis method under various test conditions were compared.

2. Principle

Unlike a small-diameter, single-hole imaging device, the coded-aperture approach uses a multi-hole mask as a collimator, which is placed in front of and parallel to the detector. Coded-aperture imaging involves encoding and decoding processes [12,31,32]. Photons emitted from the source are modulated by the coded-aperture mask and then detected by the detector. An overlapping image of the object is then recorded. The purpose of the decoding procedure is to reconstruct the recorded image to the raw image that represents the real position and shape of the object (see Fig. 1).

Uniformly redundant array (URA) [12,33] and modified uniformly redundant array (MURA) [18] based coded apertures are the two of the most commonly used apertures in gamma-ray imaging. MURA can be designed to be square-shaped or hexagonal, and has been widely used in radiation monitoring. Correlation analysis is a conventional reconstruction algorithm that uses the auto-correlation features of coded-aperture arrays. If the distribution of the transparent and opaque elements of the aperture can be represented as a binary encoding array as A and the decoding array as G, then A and G can be chosen such that the correlation of A with G approximates a delta function [1]. Thus, an ideal reconstructed image can be obtained using the correlation analysis method when the noise term is negligible. Noise can considerably affect imaging results because of limitations of imaging time and device design, thereby resulting in image degradation. In this paper, a new reconstruction method based on CNN was proposed to obtain low noise reconstructed images.

As a feedforward artificial neural network, CNN's artificial neurons can respond to a part of the coverage of surrounding elements, which enables them to perform well in image reconstruction and object recognition [23]. A CNN consists of one or more convolutional, pooling and fully connected layers, and each convolutional layer contains multiple feature maps, thereby ensure that taking advantage of the two-dimensional structure of the input is possible. Fig. 2 illustrates the basic architectures of CNN. Unlike other neural networks, the input data of CNN are two-dimensional data, and no artificial feature extraction is needed, thus simplifying the operation while retaining all the original features of the data. Two-dimensional convolution operation and pooling reduce the amount of data. The way many neurons in a given layer share the same feature map speeds up the computation. Therefore, the model training can be completed in a short time.

In this paper, the CNN includes one input layer, two convolution layers, one pooling layer, one fully connected layer, and one output layer. The number of feature maps of the two convolutional layers is 10. The size of convolution kernel in the first convolutional layer is $4 * 4$, and in the second convolutional layer is $3 * 3$. The size of the receptive fields is $17 * 17$, which is the same size as the image. The maximum pooling was used in the pooling layer, and the pooling scale is $2 * 2$. The mean square error cost function was used for training the network. The activation function is rectified linear unit (ReLU), and the output function is sigmoid function.

3. Methods

To ensure the good generalization capability of the CNN, the training data must be sufficient and diverse. The Monte Carlo method provides great convenience for obtaining a large amount of imaging samples. The proposed method mainly includes two parts: coded-aperture imaging simulation and CNN training. After a gamma camera model is constructed in PHITS, coded images in a variety of situations can be obtained by setting different source conditions and imaging time. The raw and coded images are used to train CNN. In practical application, the coded image acquired by the gamma camera is input into the trained CNN to obtain the reconstruction result (see Fig. 3).

3.1. Construction of gamma camera

The CZT detector is one of the most commonly used room temperature semiconductor detectors. It has a high energy-resolution and no refrigeration requirements, thereby making it widely used in X-ray and gamma-ray detection. CZT pixel detectors are widely used in the field of medicine and astronomy for X-ray and gamma-ray imaging [34,35]. The active area of the CZT detector employed in this paper is $25.5 \times 25.5 \times 5$ mm^3, divided into 17×17 pixels, with a single pixel size of 1.5 mm × 1.5 mm. A 33×33 array mask (a mosaic of two cycles of 17×17 MURA mask) [12,18] was used to modulate the incident photons that are stopped by CZT. The size of the single hole is the same as that of the detector pixel. The mask has a length and width of 49.5 mm while the thickness of mask and surrounding shield is 5 mm. The material of the mask is tungsten. Fig. 4 shows the 3D model of the designed gamma camera, wherein the MURA mask is parallel and center-aligned with the CZT array with a distance of 33 mm.

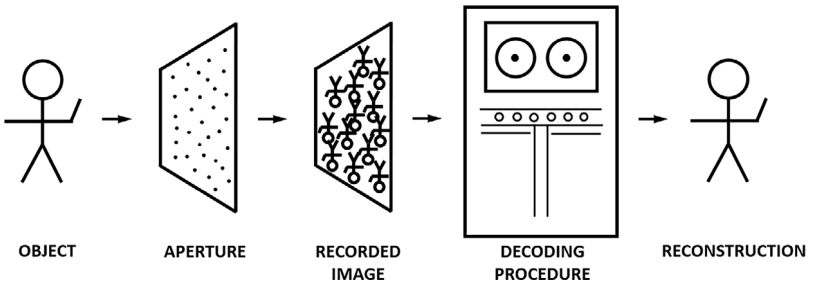

Fig. 1. Basic steps involved in coded-aperture imaging [12].

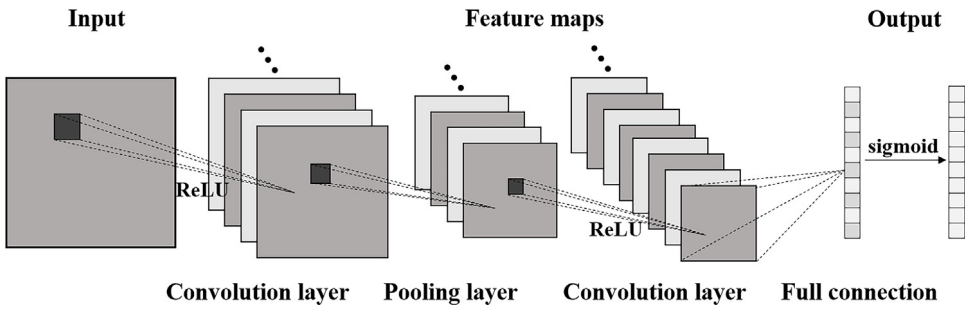

Fig. 2. Architectures of CNN.

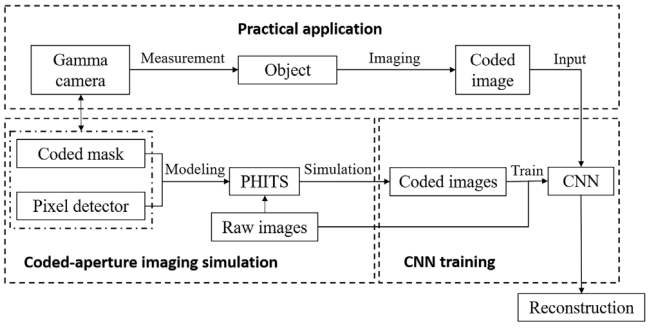

Fig. 3. Block diagram of the CNN method for coded image reconstruction.

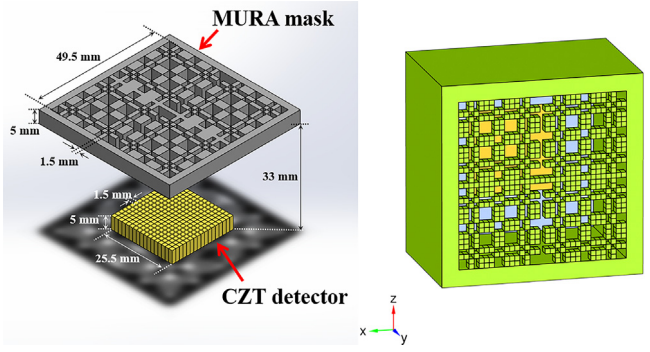

Fig. 4. On the left: schematic of rank 17 mosaic MURA mask and CZT detector. On the right: 3D model of gamma camera in PHITS.

3.2. Acquisition of simulation data and CNN training

In the training data acquisition, a Cs-137 source with a radioactivity of 3.7E7 Bq was placed 1 m away from the mask. The source was a small, isotropic cylindrical source, and the photons were approximately incident from one point to the coded mask. Coded images under different conditions can be obtained by changing the position of the sources and imaging time. An array representing the location of the radioactive source, that is, the raw image, was obtained by discretizing the detection plane into a 17×17 image, where 1 indicates the presence of a source, and 0 indicates no source. A raw image and a coded image obtained by the detector form a dataset. One to three radioactive sources in different locations were randomly set in the detection plane in each dataset. The simulation imaging time is 20 s. Fig. 5 shows the acquisition of a simulation dataset when the number of sources is 3. The total number of simulated datasets is one million. The distribution of the radioactive sources of the simulated data used in the training and verification of CNN model was randomly selected from all cases in which the number of sources was one to three, and the total number of simulated datasets was one million. All datasets were divided into two parts; 90% constitute the training set, and 10% constitute the validation set. The training and validation sets were used to tune the CNN's structure and hyperparameters such as step size, number of iterations and batch size. The code was developed and operating in MATLAB. The training of the CNN model was carried out on a 3.4 GHz CPU with the time of 50 h.

3.3. Method for evaluating reconstructed images

To illustrate the reconstruction capability of the CNN method, contrast-to-noise ratio (CNR) [36] was used to evaluate the reconstructed image ability.

CNR is used to characterize the contrast between the region of interest and the background noise of the reconstructed image. It can also be used to illustrate the ease with the location of the source can be identified directly from the reconstructed image.

$$CNR = \frac{\overline{V} - B}{\sigma} \tag{1}$$

where $\overline{V}$, B, and σ are the intensity of the signal in the region of interest, the mean value of the background, and the standard deviation of the background, respectively. In this paper, the region of interest means the pixels which correspond to the original point source locations. *CNR* is used as an index for identifying the target and the contrast of the background in the image. A large *CNR* corresponds to the easy of direct identification of the position of the source from the reconstructed

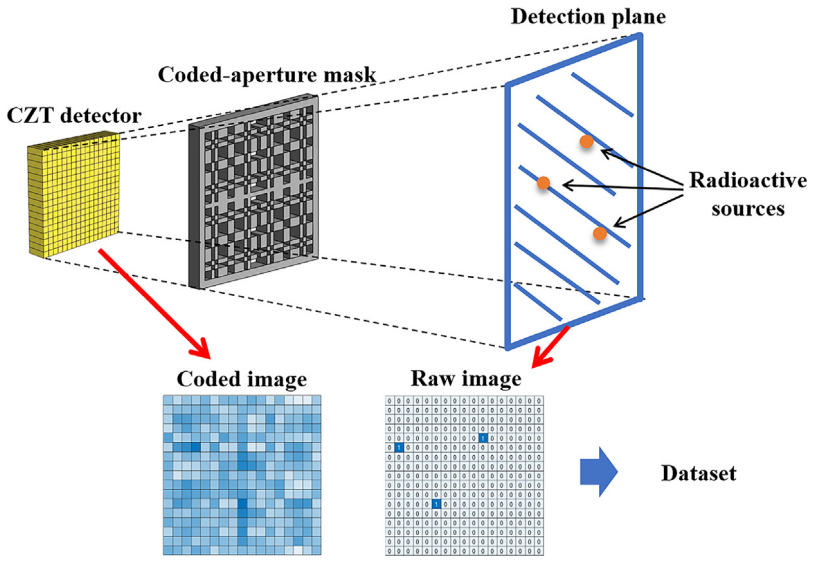

Fig. 5. Acquisition of a coded-aperture imaging simulation dataset when the number of sources is three.

image, which is important in the practical application of radioactive source search. When comparing the CNR of images obtained by the two methods, the result after using a simple numerical cut-off process is also shown (Sections 4.1 and 4.6). If *mu* is the average of pixel values and *sigma* is the standard deviation of pixel values, setting all pixel values below (*mu* + 3 × *sigma*) to zeros could maximize noise removal while preserving the signal.

4. Results and discussion

4.1. Reconstruction of single radioactive source in the field-of-view

Image reconstruction using the CNN method was simulated when the radioactive single source was located in 289 different locations within the field-of-view (FOV). A total of 289 different regions within FOV correspond to 17 × 17 pixels of the reconstructed image; in each case, a radioactive source was located in one of the regions. The imaging time was 20 s, and other conditions were the same as the training data acquisition conditions. Fig. 6 shows the CNR of the reconstructed images obtained by the CNN method and correlation analysis method. The pie chart indicates the proportion of the cases which CNR is infinite after using numerical cut-off.

For the 289 single-source cases, raw reconstruction result obtained by the CNN method have an average CNR of 177.2, and more than 69% of the values are greater than 100. The results obtained by the correlation analysis method have an average CNR of 10.6, and the values are distributed between five to twenty. After the numerical cut-off process, the CNR values of the images obtained by the two methods are greatly improved. For the CNN method, 81.07% of the 289 CNR values are infinite, and the average of the remaining CNR values is 49.3. For the correlation analysis method, only 27.68% of the 289 CNR values are infinite, and the average of the remaining CNR values is 81.3. The CNR of the image obtained by the CNN method is significantly higher than that obtained by correlation analysis method. Both methods can obtain a perfect image that the CNR value is infinite using the numerical cutoff. It is easier to obtain images without noise using the CNN method combined with numerical cutoff.

Fig. 6 also shows that the source close to the FOV center provides large CNR. When the source is located in the outermost region, a significant deviation appears between the reconstructed images and the raw image. Analysis shows that the reason for this phenomenon is that obliquely incident photons produce repeated counts in several adjacent pixels of the detector, blurring the coded image and resulting in distortion of the reconstructed images. This phenomenon can be reduced by lowering the detector thickness or setting small FOV of the gamma camera. Fig. 7 illustrates the process of this phenomenon during coded-aperture imaging, and Fig. 8 indicates that reducing the thickness of the detector can reduce artifacts. When the source is at the outermost side of FOV, artifacts appear on the opposite side, and as the source gradually approaches the center of FOV, artifacts appear in adjacent pixels and the intensity gradually decreases. In the design of gamma cameras, the trade-off between detector thickness and photon diffusion should be considered in the design of gamma cameras.

4.2. Reconstruction of radioactive source with different distances and imaging time

When the radioactive point source is located at different distances from the gamma camera, the images with different imaging time were reconstructed by using the CNN and the correlation analysis methods. Fig. 9 shows the CNR values of reconstructed images under different conditions, and the value is the average of the CNR values of the 20 images in each condition. A Cs-137 source with a radioactivity of 3.7E7 Bq is located at different distances (0.5, 1, 2, 3, 4, and 5 m) and with different imaging times (5, 10, 20, 30, 40 and 50 s).

In most cases, CNR of images reconstructed by using the CNN method is generally much larger than that of the images reconstructed by using the correlation analysis method. However, when the source is 2, 3, 4 and 5 m from the camera and the measurement time is 5 and 10 s, the CNR of the reconstructed images obtained by the CNN method is very low, indicating that the reconstructed image is completely distorted.

For the two methods, the CNR of the reconstructed image of the source gradually increases with the increase in the measurement time when the distance between the source and the camera is fixed. However, the increase of CNR is not obvious after a certain imaging time is reached because the randomness of data and noise is reduced at a sufficient imaging time. When the measurement time is fixed, the CNR of the reconstructed image gradually decreases, as the distance between the source and the camera increases. This trend can be explained by a theoretical model of coded-aperture imaging. Suppose a total of N photons strike the coded mask from a single point source, and assume that the mask is 100% opaque to photons and that the detector also has 100% detection efficiency. Then, because half of the mask pixels are holes, the brightness of the reconstructed point source will be $(1/2)N$, while the brightness of the background pixels will by $(1/4)N$, and being

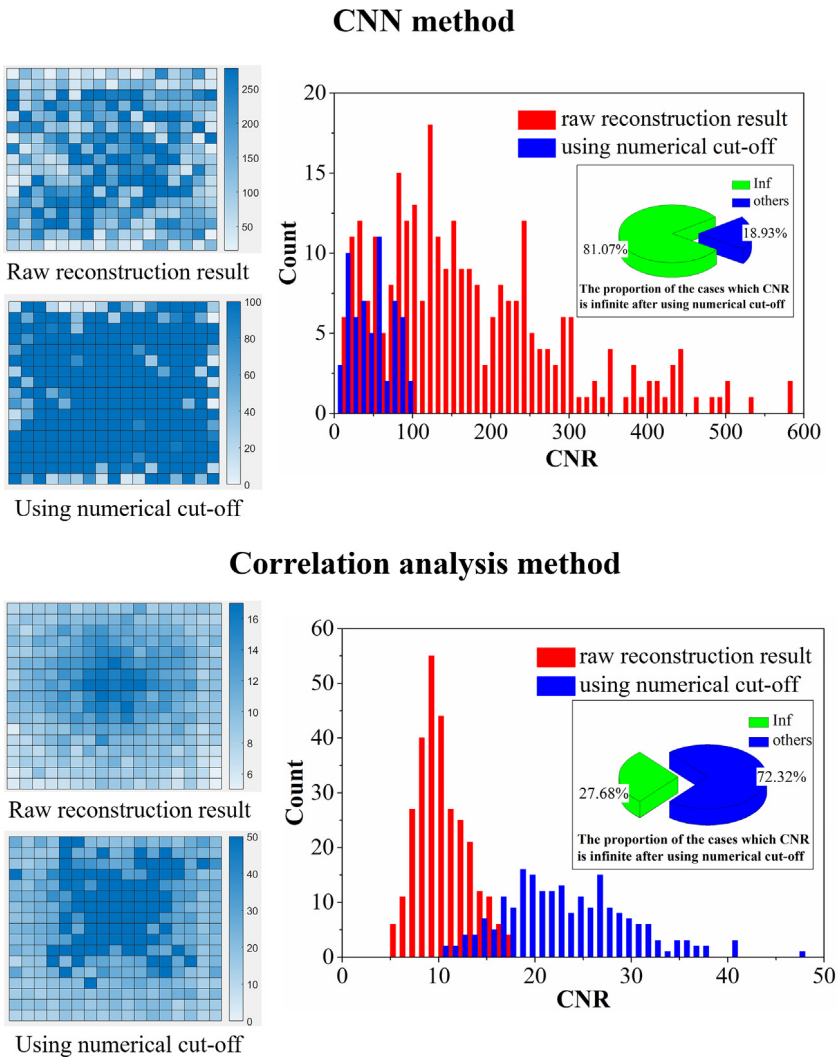

Fig. 6. CNR of 289 reconstructed images using the CNN and the correlation analysis method.

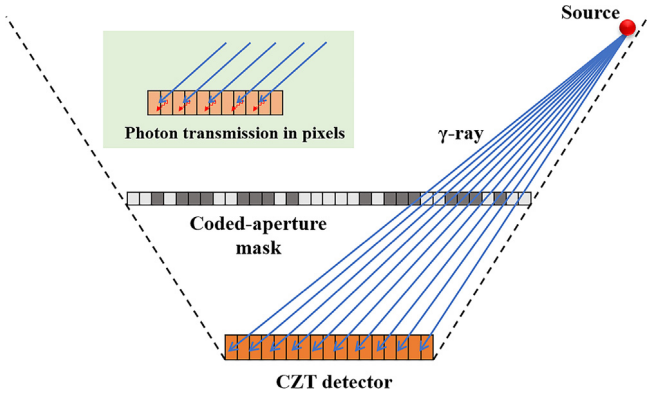

Fig. 7. Transmission of photons in the detector when the source is at the edge of the FOV.

Poisson variables their variance will be the same $(1/4)N$, and hence their standard deviation will be $sqrt\{(1/4)N\}$. So the CNR is expected to be $\{(1/2)N - (1/4)N\}/sqrt\{(1/4)N\} = (1/2)sqrt\{N\}$. Since N is proportional to the imaging time T, and inversely proportional to the square of the distance from the source to the detector D, this means that the CNR will be proportional to $sqrt\{T\}/D$. This is exactly what shown in Fig. 9 that the CNR values increase like sqrt{T}, while decrease like 1/D. When the source is very close to the camera (0.5 m), the CNR value of images obtained by correlation analysis method is significantly reduced. This is due to the artifacts caused by variations in the size of the mask shadow, which is shown in Fig. 10.

Fig. 10 shows the reconstruction results obtained by the two methods for different imaging time and distances, and the reconstructed image quality shows the same trend as CNR. When the signal strength is high (with the long imaging time and short distance), both methods can reconstruct the actual position of the sources well, and the images

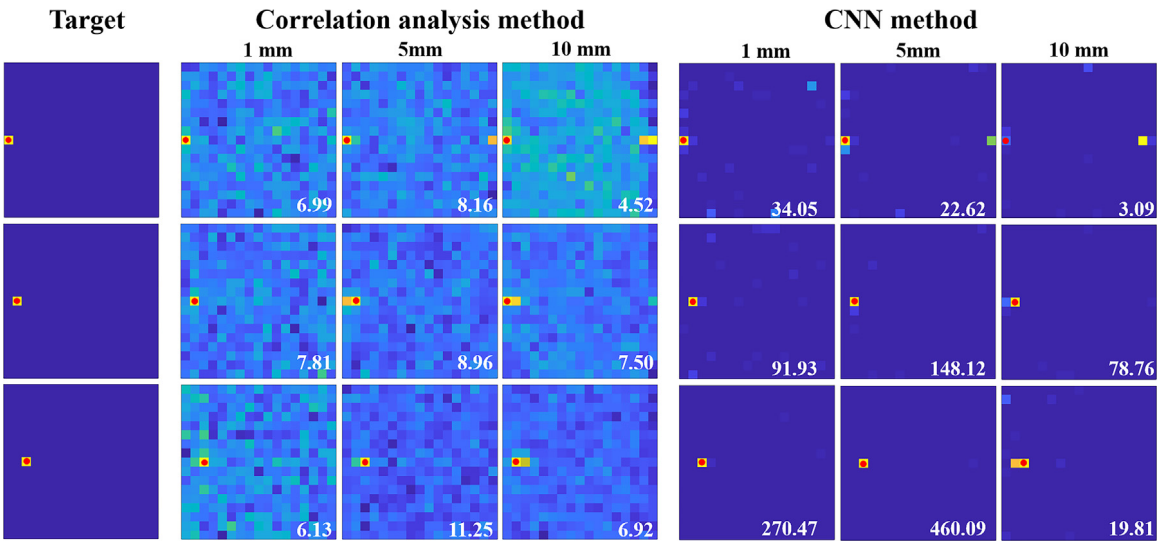

Fig. 8. Reconstructed images of the source at the edge of FOV at different detector thicknesses (1 mm, 5 mm, 10 mm). The red dots indicate the actual location of the sources.

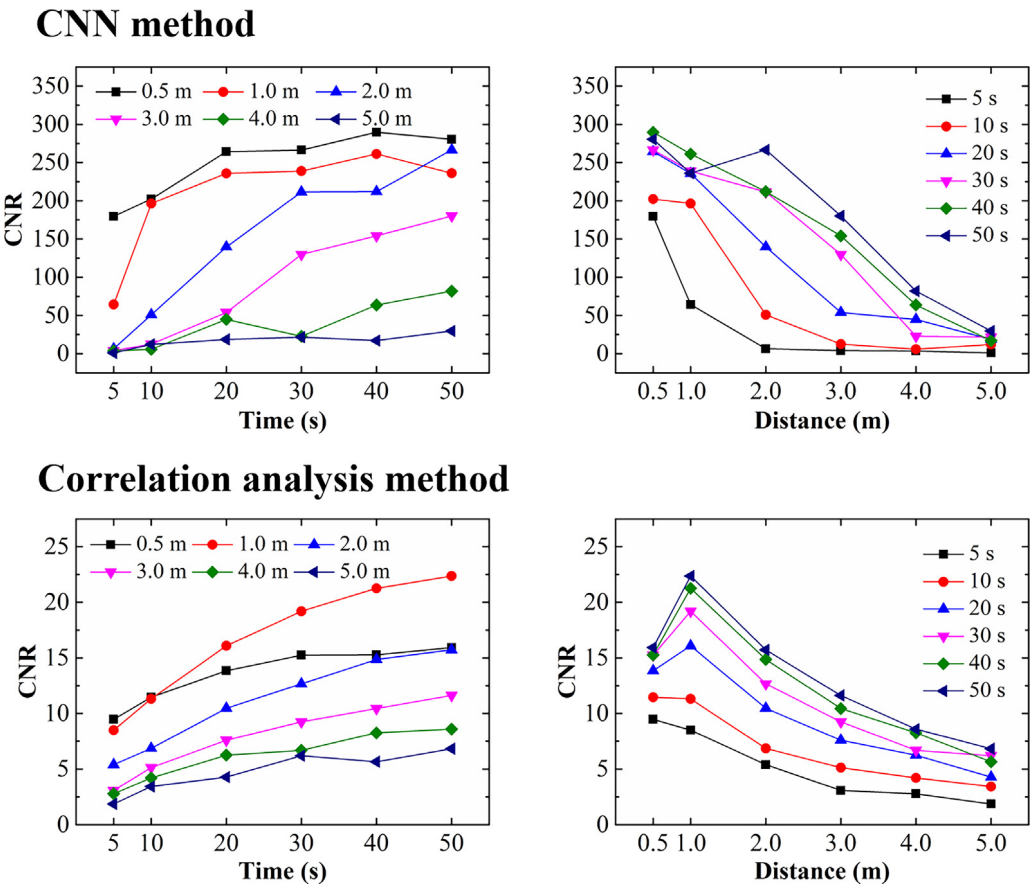

Fig. 9. CNR of reconstructed images using the CNN (top row) and the correlation analysis (bottom row) methods.

obtained by the CNN method are purer. In the cases where the distance is 0.5 m or the distance is 1 m and the imaging time is greater than 20 s, artifacts shown in the images obtained by correlation analysis method do not appear in the reconstructed images obtained by the CNN method, which means that the CNN method has the ability to remove the inherent noise caused by geometry. When the signal strength is low (with the short imaging time and long distance), both methods fails to indicate the true position of the source. The effective signal of the reconstructed image obtained by the correlation analysis method is progressively overwhelmed as the noise increases, while the image reconstructed by the CNN method gives a completely wrong signal position. In low flux conditions, correlation analysis method has the advantage that it indicates uncertainly where the source may exist, whereas the CNN method continues to give an unambiguous location for the point source, but a location that may simply be flat wrong.

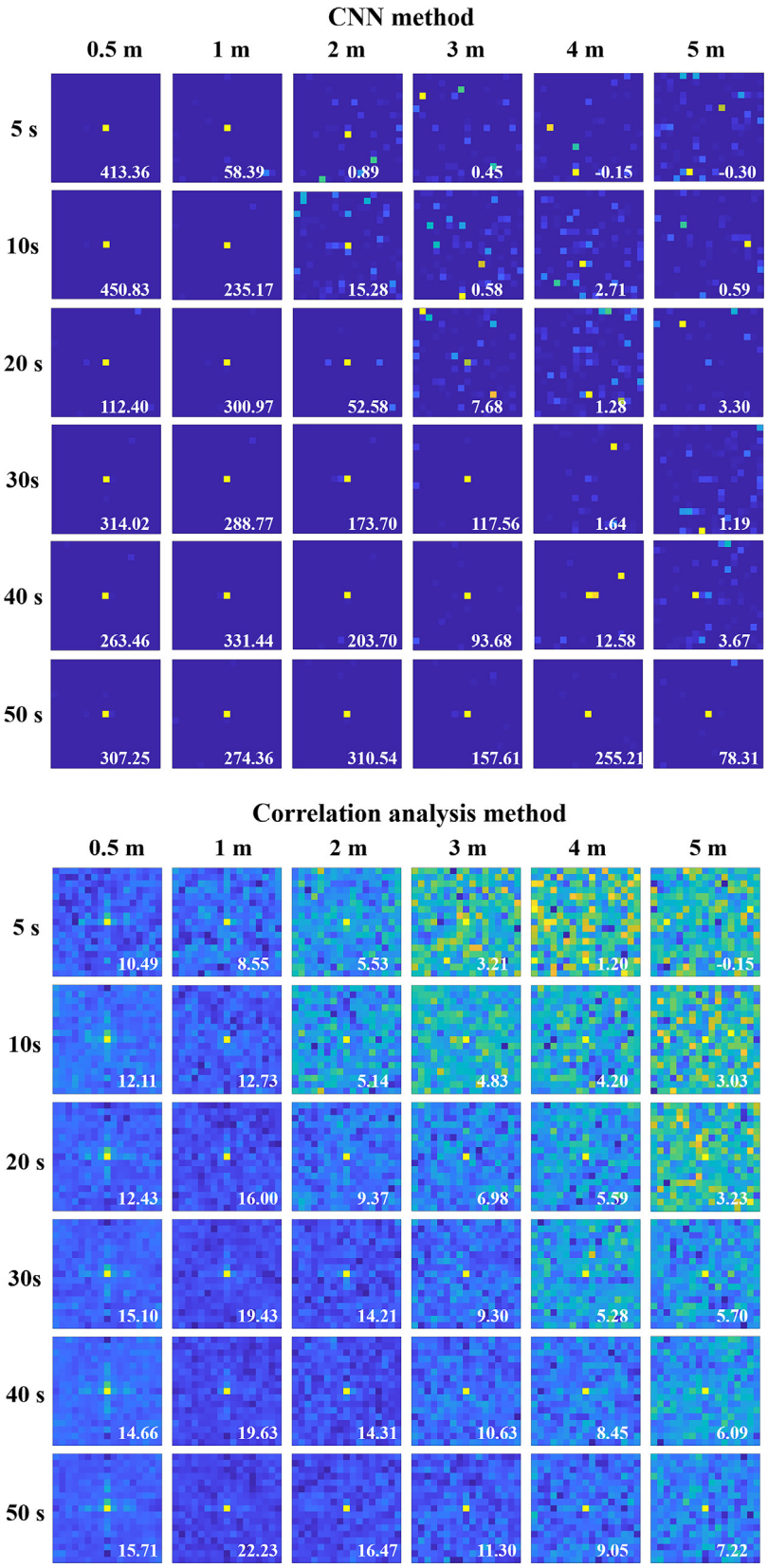

Fig. 10. Reconstructed images of different cases using the CNN and correlation analysis method (with CNR at the bottom right corners).

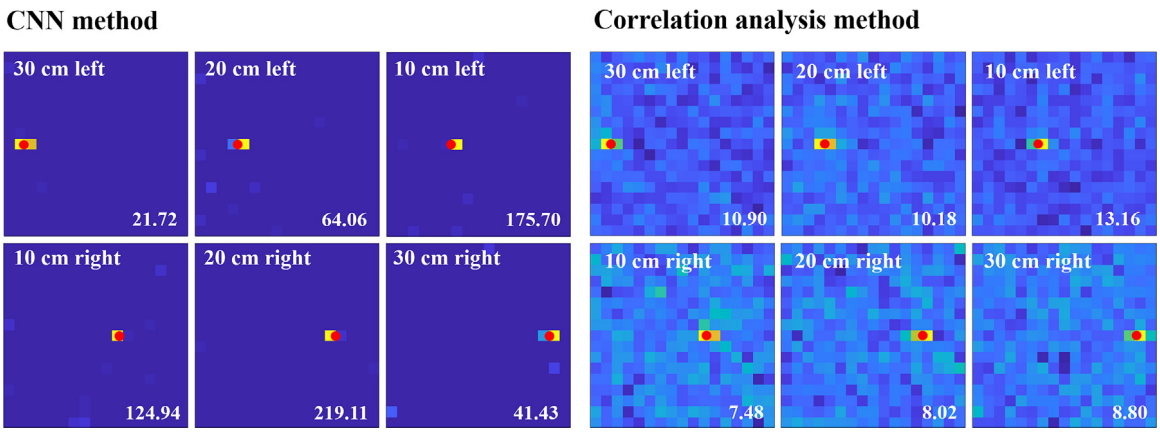

Fig. 11. Reconstructed image of the source at different locations from the center using the CNN (left) and the correlation analysis (right) methods (with CNR at the bottom right corners). The red dots indicate the actual location of the sources.

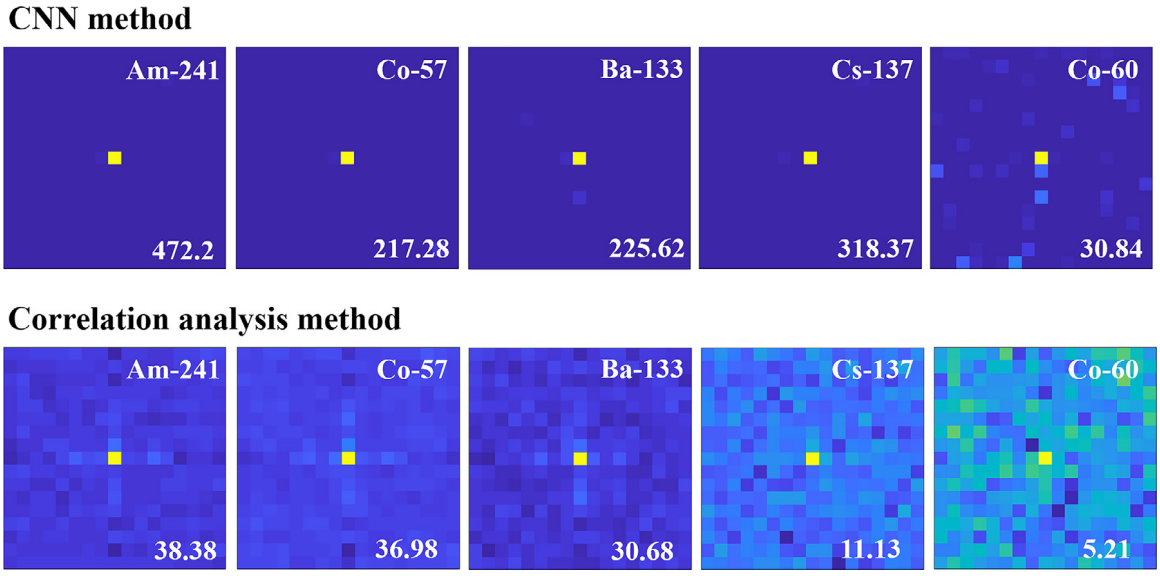

Fig. 12. Reconstructed images of different types of radioactive sources using the CNN (top row) and the correlation analysis (bottom row) methods (with CNR at bottom right corners).

4.3. Reconstruction of radioactive source with different positions in the offset center of FOV

The imaging performance of gamma cameras is greatly affected by the transmission and scattering process of photons in the coded-aperture mask. When a photon is obliquely incident through the mask, the image may be blurred due to the difference of photon track in the mask. The imaging performance of the CNN method was evaluated with a Cs-137 source with a radioactivity of 3.7E7 Bq located 10, 20, and 30 cm from the outer margin with an imaging time of 20 s.

Fig. 11 shows that the images obtained by CNN method can accurately distinguish the position of the source when the source is off the center of FOV. The source was located at the edge of the pixel, so that adjacent pixel near the source was activated in the reconstructed image. In all cases, the CNR of the results of the CNN method is higher than that of the results of the correlation analysis method. The image obtained by correlation analysis method tends to activate two adjacent pixels at the same time, and the image obtained by the CNN method is biased toward one of the pixels.

4.4. Reconstruction of radioactive sources with different energy

In this paper, Cs-137 was used as the source of the CNN model training data acquisition. To study the applicability of different kinds of radioactive sources under the designed camera and CNN method, the reconstructions of several radioactive sources are compared. The distance between the source and camera is 1 m, the source activity is 3.7E7 Bq and the imaging time is 10 s. Four common industrial and medical radioactive sources (Am-241, Co-57, Ba-133, Cs-137, Co-60) are shown in Fig. 12. These source names and their primary gamma ray energy (Am-241, Co-57, Cs-137, Co-60) or average gamma ray energy (Ba-133) are given in the upper right corner of the images. The results show that the CNN method can provide a purer reconstructed image and a higher CNR value than the correlation analysis method. As the photon energy increases, the quality of images obtained by correlation analysis method gradually decreases, while the image obtained by the CNN method shows significant noise only under Co-60 source. In the case where the source energy is low, the reconstructed image obtained by correlation analysis method exhibits the artifact as shown in Fig. 10, which is because when low-energy photons have weaker penetrability, the variations in the size of the mask shadow become significant.

4.5. Reconstruction of multiple radioactive sources

In radioactive source supervision in customs ports and the identification of radiation pollution after nuclear accidents, accurate identification of multiple radioactive sources at the same time is an important

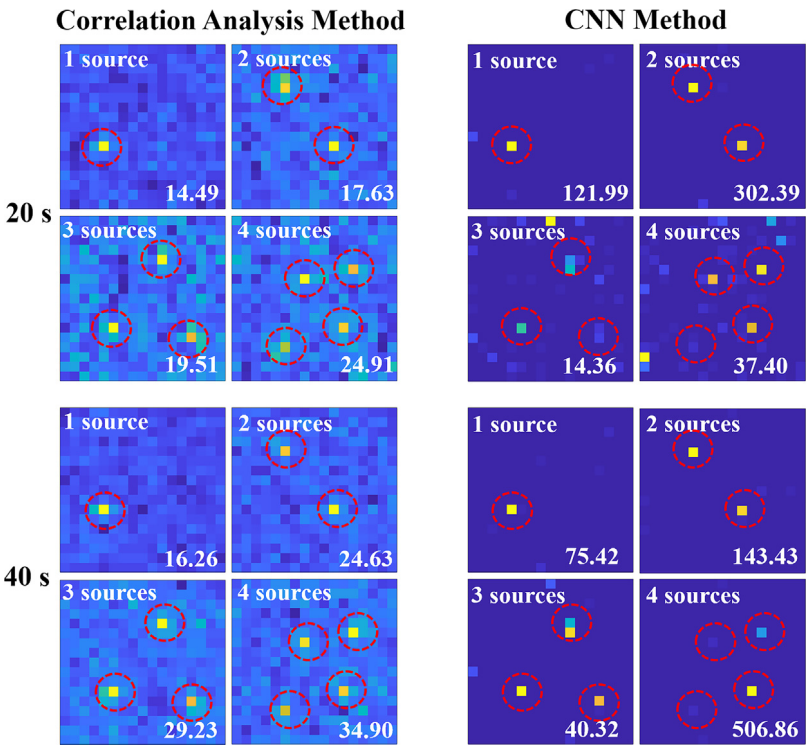

Fig. 13. Reconstructed images of different numbers of radioactive sources using the CNN (right column) and the correlation analysis methods (left column) with different times (20 s, 40 s). The red cycles indicate the actual location of sources.

aspect of the performance of gamma cameras. A simulation that uses one to four radioactive sources was conducted. The Cs-137 sources with activity of 3.7E7 Bq was located 1 m away from the camera, and the imaging time was 20 s and 40 s.

Fig. 13 shows that the reconstructed images obtained by the CNN method have a higher quality than those obtained by the correlation analysis method in the presence of only one to two radioactive sources. However, the reconstructed images are blurred when three to four radioactive sources exist simultaneously. The values of the pixels corresponding to the regions where the sources are located are different despite the sources have the same activity. These weak signals may be judged as noise or artifacts when the number of radioactive sources is unknown. This phenomenon becomes significant as the number of sources increases because the CNN training data cover only the case with fewer than four radioactive sources; poor performance is observed with more than three sources. This problem can be solved by expanding the training set with a simulation dataset with more sources. No similar phenomena occurred with the results obtained by the correlation analysis method; however, as the number of sources increases, the background noise increases and the image quality deteriorates. Therefore, the use of a threshold to artificially distinguish the region of interest and background to provide guidance for practical work is necessary.

4.6. Overall testing of trained CNN

Ten thousand simulated datasets, which are different from the training and validation set, were selected to test the reconstruction effectiveness of the CNN and the correlation analysis methods. Fig. 14 shows the CNR of the raw reconstruction results obtained by the two methods and the CNR of the results using the numerical cut-off. The pie chart indicates the proportion of the cases which CNR is infinite after using numerical cut-off.

Raw reconstruction results obtained by the CNN method have an average CNR of 169.08, and more than 58.48% of the values are greater than 100. The results obtained by the correlation analysis method have an average CNR of 16.04, and the values are distributed between zero to thirty. After the numerical cut-off process, the CNR values of the images obtained by the two methods are greatly improved. For the CNN method, 61.86% of the ten thousand CNR values are infinite, and the average of the remaining CNR values is 46.6. For the correlation analysis method, only 4.69% of the ten thousand CNR values are infinite, and the average of the remaining CNR values is 49.99. The CNR of the image obtained by the CNN method is significantly higher than that obtained by correlation analysis method.

5. Conclusion

This paper presented a CNN-based reconstruction method for coded-aperture imaging to improve the quality of reconstructed images and the accuracy of source location recognition with a short imaging time under low count conditions. A compact gamma camera based on CZT pixel detector and MURA mask was constructed to study the effectiveness of the CNN method in image reconstruction under various conditions. Simulation results show that the trained CNN can be used in the reconstruction process of coded images, and can effectively reduce image noise. The CNR of the images obtained by the CNN method was large than that obtained by correlation analysis method. After using the numerical cut-off, the CNR of the reconstructed images obtained by the two methods was significantly improved, and the CNN method was easier to obtain a perfect image without noise. In addition, the CNN method shows the great potential to remove artifacts caused by non-parallel rays. However, when the photon flux was low, the CNN method may fail catastrophically giving completely wrong source position.

When the imaging time is the same, the proposed method can suppress the noise well and obtain a reconstructed image with better image quality. At the same time, the time consumption of the CNN method is mainly concentrated in the training phase; in practical application, time-consuming operations such as iteration are not needed. Thus, the method can be used for real-time measurement and dynamic monitoring of radioactive sources, and has great application potential in the field of orphan source search, monitoring of radioactive sources,

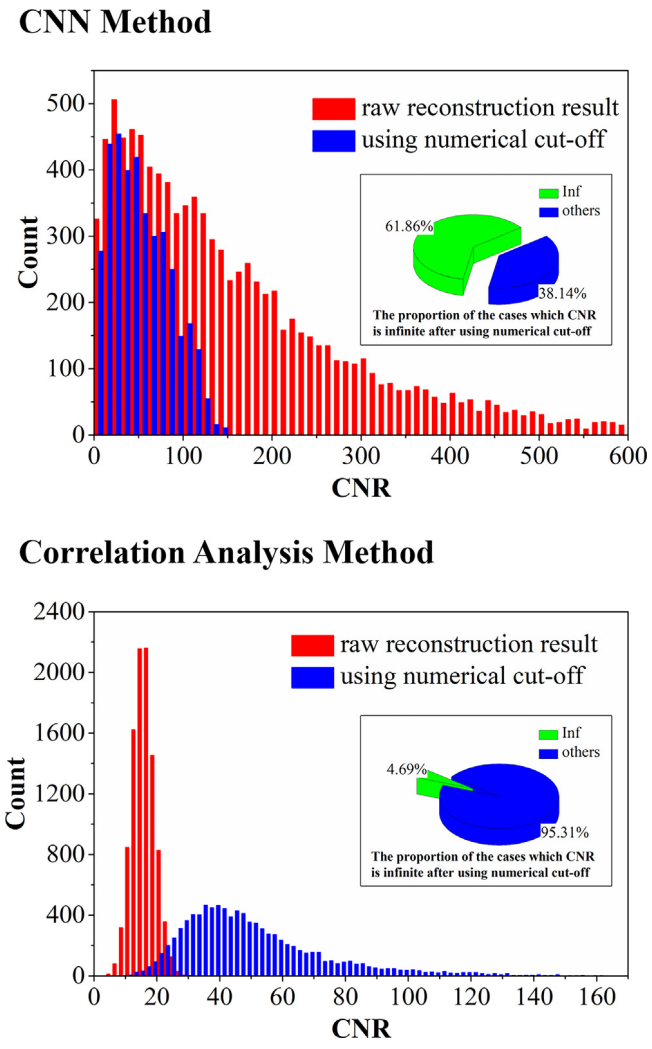

Fig. 14. CNR of reconstructed images using the CNN (top) and the correlation analysis methods (bottom).

and detecting illicit nuclear material, which require fast and accurate radioactive source positioning capability. Furthermore, the CNN method is not specific to a certain coded-aperture array and can be extended to other aperture arrays, such as random array, URA array, and hexagonal MURA array. For a specific scenario, this method can accurately model the environment which can improve the performance.

In addition, the CNN method is less effective when multiple sources are simultaneously present because as the number of sources increases, all possible cases of sources position increase geometrically, and completely covering all situations by a training set is difficult. Further research can be conducted using unsupervised learning methods or other neural network models.

Acknowledgments

This work was supported by the National Natural Science Foundation of China (Grant No. 11675078), the Primary Research and Development Plan of Jiangsu Province, China (Grant No. BE2017729), the Fundamental Research Funds for the Central Universities, China (Grant No. NJ20160034), the Postgraduate Research & Practice Innovation Program of Jiangsu Province, China (Grant No. KYLX16_0353), and the Foundation of Graduate Innovation Center in NUAA, China (Grant No. kfjj20180601).

References

[1] M.J. Cieślak, K.A.A. Gamage, R. Glover, Coded-aperture imaging systems: Past, present and future development–A review, Radiat. Meas. 92 (2016) 59–71.
[2] K.P. Ziock, L. Fabris, D. Carr, J. Collins, M. Cunningham, F. Habte, T. Karnowski, W. Marchant, A fieldable-prototype, large-area, gamma-ray imager for orphan source search, IEEE Trans. Nucl. Sci. 55 (2008) 3643–3653.
[3] M. Eisenbud, T.F. Gesell, Environmental Radioactivity from Natural, Industrial and Military Sources: From Natural, Industrial and Military Sources, fourth ed., Academic Press, London, 1997.
[4] P. Fracas, J.P. Gayral, G. Krishnamachari, M.S. Kale, P. Chaudhury, K.S. Pradeepkumar, D.N. Sharma, R. Venkat, R.S. Deshpande, Methodologies and systems to meet the challenges of locating and recovering orphan sources: source search operation conducted by French and Indian teams in the Republic of Georgia, in: Secur. Radioact. Sources. Proc. an Int. Conf., 2003.
[5] M. Laraia, Nuclear Decommissioning: Planning, Execution and International Experience, Woodhead Publishing, Cambridge, 2012.
[6] P.T. Durrant, M. Dallimore, I.D. Jupp, D. Ramsden, The application of pinhole and coded aperture imaging in the nuclear environment, Nucl. Instrum. Methods Phys. Res. A 422 (1999) 667–671.
[7] O. Gal, M. Gmar, O.P. Ivanov, F. Lainé, F. Lamadie, C. Le Goaller, C. Mahé, E. Manach, V.E. Stepanov, Development of a portable gamma camera with coded aperture, Nucl. Instrum. Methods Phys. Res. A 563 (2006) 233–237.
[8] S. Sun, Z. Zhang, L. Shuai, D. Li, Y. Wang, Y. Liu, X. Huang, H. Tang, T. Li, P. Chai, Development of a panorama coded-aperture gamma camera for radiation detection, Radiat. Meas. 77 (2015) 34–40.
[9] M. Gmar, M. Agelou, F. Carrel, V. Schoepff, GAMPIX: A new generation of gamma camera, Nucl. Instrum. Methods Phys. Res. A 652 (2011) 638–640.
[10] S. Sun, Z. Zhang, L. Shuai, D. Li, Y. Wang, Y. Liu, X. Huang, H. Tang, T. Li, P. Chai, Far field 3D localization of radioactive hot spots using a coded aperture camera, Appl. Radiat. Isot. 107 (2016) 177–182.
[11] M. Gmar, O. Gal, C. Le Goaller, O.P. Ivanov, V.N. Potapov, V.E. Stepanov, F. Laine, F. Lamadie, Development of coded-aperture imaging with a compact gamma camera, IEEE Trans. Nucl. Sci. 51 (2004) 1682–1687.
[12] E.E. Fenimore, T.M. Cannon, Coded aperture imaging with uniformly redundant arrays, Appl. Opt. 17 (1978) 337–347.
[13] J.G.M. FitzGerald, A rotating scatter mask for inexpensive gamma-ray imaging in orphan source search: Simulation results, IEEE Trans. Nucl. Sci. 62 (2015) 340–348.
[14] P.M.E. Shutler, A. Talebitaher, S.V. Springham, Signal-to-noise ratio in coded aperture imaging, Nucl. Instrum. Methods Phys. Res. A 669 (2012) 22–31.
[15] R.H. Dicke, Scatter-hole cameras for x-rays and gamma rays, Astrophys. J. 153 (1968) L101.
[16] A. Zoglauer, M. Galloway, M. Amman, S.E. Boggs, J.S. Lee, P.N. Luke, L. Mihailescu, K. Vetter, C.B. Wunderer, First results of the high efficiency multimode imager (HEMI), in: Nucl. Sci. Symp. Conf. Rec. (NSS/MIC), 2009 IEEE, IEEE, 2009, pp. 887–891.
[17] A. Zoglauer, M. Galloway, M. Amman, P.N. Luke, S.E. Boggs, Aerial standoff detection with the high efficiency multimode imager (HEMI), in: Nucl. Sci. Symp. Conf. Rec. (NSS/MIC), 2010 IEEE, IEEE, 2010, pp. 566–570.
[18] S.R. Gottesman, E.E. Fenimore, New family of binary arrays for coded aperture imaging, Appl. Opt. 28 (1989) 4344–4352.
[19] S. Berrim, A. Lansiart, J.-L. Moretti, Implementing of maximum likelihood in tomographical coded aperture, in: Proc. 3rd IEEE Int. Conf. Image Process., IEEE, 1996, pp. 745–748.
[20] T.J. Ponman, Maximum entropy methods, Nucl. Instrum. Methods Phys. Res. 221 (1984) 72–76.
[21] F.J. Ballesteros, F.S. Martínez, V.R. Velasco, The EM imaging reconstruction method in γ-ray astronomy, Nucl. Instrum. Methods Phys. Res. B 145 (1998) 469–481.
[22] Z. Mu, Y.-H. Liu, Aperture collimation correction and maximum-likelihood image reconstruction for near-field coded aperture imaging of single photon emission computerized tomography, IEEE Trans. Med. Imaging 25 (2006) 701–711.
[23] G.E. Hinton, R.R. Salakhutdinov, Reducing the dimensionality of data with neural networks, Science (80-.) 313 (2006) 504–507.
[24] P. Olmos, J.C. Diaz, J.M. Perez, G. Garcia-Belmonte, P. Gomez, V. Rodellar, Application of neural network techniques in gamma spectroscopy, Nucl. Instrum. Methods Phys. Res. A 312 (1992) 167–173.
[25] J. He, X. Tang, P. Gong, P. Wang, L. Wen, X. Huang, Z. Han, W. Yan, L. Gao, Rapid radionuclide identification algorithm based on the discrete cosine transform and BP neural network, Ann. Nucl. Energy 112 (2018) 1–8.
[26] J. He, X. Tang, P. Gong, P. Wang, Z. Han, W. Yan, L. Gao, Spectrometry analysis based on approximation coefficients and deep belief networks, Nucl. Sci. Technol. 29 (2018) 69.
[27] F.J. Ballesteros, E.M. Muro, B. Luque, Speeding up image reconstruction methods in coded mask γ cameras using neural networks: Application to the EM algorithm, Exp. Astron. 11 (2001) 207–222.
[28] L. Xu, J.S.J. Ren, C. Liu, J. Jia, Deep convolutional neural network for image deconvolution, in: Adv. Neural Inf. Process. Syst., 2014, pp. 1790–1798.
[29] M. Hradiš, J. Kotera, P. Zemcík, F. Šroubek, Convolutional neural networks for direct text deblurring, in: Proc. BMVC, 2015, p. 2.

[30] L. Sihver, D. Mancusi, T. Sato, K. Niita, H. Iwase, Y. Iwamoto, N. Matsuda, H. Nakashima, Y. Sakamoto, Recent developments and benchmarking of the PHITS code, Adv. Sci. Res. 40 (2007) 1320–1331.
[31] P.M.E. Shutler, S.V. Springham, A. Talebitaher, Mask design and fabrication in coded aperture imaging, Nucl. Instrum. Methods Phys. Res. A 709 (2013) 129–142.
[32] P.M.E. Shutler, S.V. Springham, A. Talebitaher, Periodic wrappings in coded aperture imaging, Nucl. Instrum. Methods Phys. Res. A 738 (2014) 132–148.
[33] E.E. Fenimore, Coded aperture imaging: the modulation transfer function for uniformly redundant arrays, Appl. Opt. 19 (1980) 2465–2471.
[34] M. McCleskey, W. Kaye, D.S. Mackin, S. Beddar, Z. He, J.C. Polf, Evaluation of a multistage CdZnTe compton camera for prompt γ imaging for proton therapy, Nucl. Instrum. Methods Phys. Res. A 785 (2015) 163–169.
[35] J. Grindlay, J. Hong, B. Allen, S. Barthelmy, R. Baker, Development of tiled imaging CZT detectors for sensitive wide-field hard X-ray surveys to EXIST, Nucl. Instrum. Methods Phys. Res. A 652 (2011) 671–673.
[36] R.E. Hendrick, Signal, noise, signal-to-noise, and contrast-to-noise ratios, Breast MRI Fundam. Tech. Asp. (2008) 93–111.